MIMO Transmission over High Delay Spread Channels with Reduced Cyclic Prefix Length

Erich Zöchmann, Stefan Pratschner, Stefan Schwarz and Markus Rupp
Institute of Telecommunications
TU Wien
1040 Vienna, Austria
Email: {ezoechma,spratsch,sschwarz,mrupp}@nt.tuwien.ac.at

***Abstract*—In 3GPP LTE communication systems, the physical layer is based on Orthogonal Frequency-Division Multiple Access and Single Carrier Frequency-Division Multiple Access in the downlink and uplink, respectively. For both schemes two different cyclic prefix (CP) lengths are standardized, a normal CP length and an extended version, the latter being intended for high delay spread channels. We retain the simple one tap equalizer and show that appropriate adaptation of the modulation and coding scheme, rather than extending the CP, yields better throughputs in a typical SNR regime of operation. The proposed adaptation takes the effects of the intersymbol (ISI) and intercarrier (ICI) interference into account, where the ISI/ICI is modelled as coloured noise, which degrades the SNR, and therefore directly affects the feedback parameters.**

***Keywords*—LTE-A, SC-FDMA, OFDMA , CP length, limited feedback, MBSFN**

I. Introduction

As a result of multipath propagation in a wireless communication system, high delay echos may occur due to scattering objects in great distance, as depicted in Figure 1a. A prominent channel model for such scenarios is the hilly terrain (HT) channel [1]. On the other hand, high delay copies of the transmit signal can also originate from the deployment of a single frequency network (SFN), as shown in Figure 1b. SFNs are currently of particular interest in the context of multimedia broadcast/multicast single frequency networks (MBSFN) [2] and HetNets [3].

In an SFN, multiple cells transmit multicast or broadcast data simultaneously and at the same frequency. The SFN transmission appears to the user equipment (UE) as a transmission from a single large cell, without any inter-cell interference. Although transmissions in an SFN are synchronized in order to avoid intersymbol interference (ISI), a user will experience different propagation delays from different base stations (BS). If the difference in delay exceeds the cyclic prefix (CP) length of an OFDM system, ISI and intercarrier interference (ICI) will occur. In rural scenarios where the cell density is sparse, the transmission of some BS may not lie inside the CP.

We use the HT channel model for our simulations. By employing a standardized channel model, we assure that our results are easy to reproduce. Figure 2 shows the HT power delay profile. We interpret the first cluster of channel taps to belong to the channel impulse response (CIR) of the near BS and the second cluster to belong to the far BS (which would be approximately $15\mu\text{s} \cdot 3 \cdot 10^5 \frac{\text{km}}{\text{s}} = 4.5\text{km}$ away).

We model the occurring ISI/ICI as additional coloured noise in order to adapt the modulation and coding scheme (MCS). Several authors have already investigated the trade-off between CP length and the Bit Error Ratio [4], [5]. Based on that findings we will show that it is beneficial - for the sake

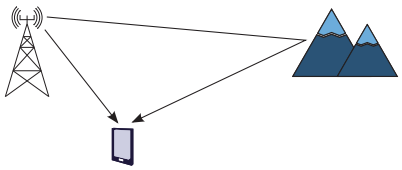

(a) A large cell in a rural area.

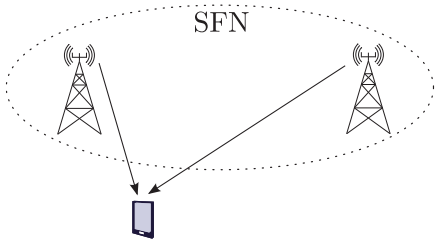

(b) A single frequency network.

Fig. 1: Examples for high delay spread environments.

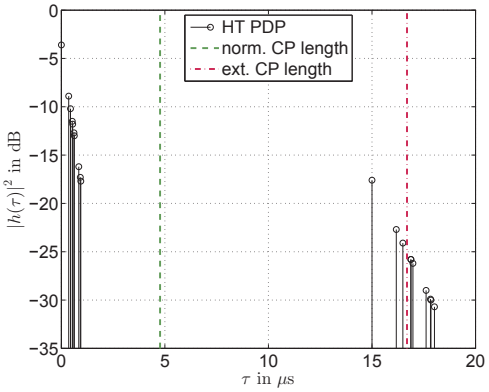

Fig. 2: HT power delay profile as prototype for SFN interference.

This work has been funded by A1 Telekom Austria AG and the Institute of Telecommunications, TU Wien.

ISBN 978-3-8007-3662-1

of *throughput* enhancement - to use shorter CP lengths and to account for the occurring ISI/ICI in the transmission rate adaptation. Especially in a scenario with high channel delay spread this is therefore an alternative strategy to extending the CP length, which implies a reduction of the payload size, i.e., a capacity loss.

Notation: Bold uppercase letters denote matrices such as $\boldsymbol{X}$ and bold lower case letters denote vectors such as $\boldsymbol{x}$. Square brackets denote the entry, of the row and column respectively, e.g., $\boldsymbol{h}[k], \boldsymbol{H}[k,n]$. We use the superscripts $(\cdot)^*$, $(\cdot)^T$, $(\cdot)^H$ for complex conjugate, transposition and conjugate transposition, respectively. $\|\cdot\|_F$ symbolizes the Frobenius norm, the entrywise (Hadamard) product is denoted by $\odot$ and the Kronecker product is denoted by $\otimes$. The all ones vector/matrix is denoted as $\mathbb{1}$. The operator $\boldsymbol{X} = \mathrm{Diag}(\boldsymbol{x})$ places the vector $\boldsymbol{x}$ on the main diagonal of $\boldsymbol{X}$ and conversely the operator $\boldsymbol{x} = \mathrm{diag}(\boldsymbol{X})$ returns the vector $\boldsymbol{x}$ from the main diagonal of $\boldsymbol{X}$. The operator $\boldsymbol{X} = \mathrm{Toeplitz}(\boldsymbol{x})$ yields a lower triangular Toeplitz structured matrix $\boldsymbol{X}$ with vector $\boldsymbol{x}$ at the first column,

$$\begin{pmatrix} x_1 & & 0 \\ \vdots & \ddots & \\ x_m & & x_1 \\ & \ddots & \vdots \\ 0 & & x_m \end{pmatrix} = \mathrm{Toeplitz}(\boldsymbol{x}) \ ,$$

with $\boldsymbol{x} = (x_1, \ldots, x_m)^T$. A block-wise Toeplitz (circulant, diagonal) matrix is a block matrix with each matrix of Toeplitz (circulant, diagonal) shape. The size of the identity matrix $\boldsymbol{I}$ and the DFT matrix $\boldsymbol{D}$ is expressed via their subscripts.

II. System Model and SNR

We consider a 3GPP LTE-A transmission system, which employs OFDMA and Single Carrier Frequency-Division Multiple Access (SC-FDMA) on the physical layer in the downlink and uplink, respectively. In order to adapt the transmission to the current channel state, LTE-A applies quantized/limited feedback, where [6] has shown that losses due to absence of full channel state information are negligible.
SC-FDMA can be described as pre-spreaded OFDM, cf. Fig. 3. In this section, we will derive a MIMO SC-FDMA system model with N_R receive antennas and N_T transmit antennas, similar to [7] for a channel which stays constant during one OFDM symbol. The LTE-A downlink system model is then a special case, where the pre-spreading is omitted.

Transmitter

The data vector $\boldsymbol{x}_l \in \mathbb{C}^{N_{SC}\times 1}$ of layer $l \in \{1, \ldots, L\}$ contains modulated symbols for each of the N_{SC} subcarriers. The number of transmit layers depends on the LTE-A specific rank indicator (RI) feedback. The data symbols are coded with a punctured turbo code whose rate is determined by the channel quality indicator (CQI), another feedback parameter. Subsequently, the codewords are mapped onto a QAM alphabet, where the size of the alphabet depends on the CQI as well. The CQI thus adapts the MCS.

When stacked into one supervector $\boldsymbol{x} \in \mathbb{C}^{N_{SC}L\times 1}$, the action of the layer wise DFT spreading is described by

$$\boldsymbol{x}' = (\boldsymbol{I}_L \otimes \boldsymbol{D}_{N_{SC}})\, \boldsymbol{x} \ . \tag{1}$$

For the joint precoding of all subcarriers we further multiply $\boldsymbol{x}$ with the precoding matrix $\boldsymbol{W} \in \mathbb{C}^{N_T\times L}$ to arrive at

$$\begin{aligned} \boldsymbol{x}'' &= (\boldsymbol{W} \otimes \boldsymbol{I}_{N_{SC}})\, \boldsymbol{x}' \\ &= (\boldsymbol{W} \otimes \boldsymbol{I}_{N_{SC}})\, (\boldsymbol{I}_L \otimes \boldsymbol{D}_{N_{SC}})\, \boldsymbol{x} \\ &= (\boldsymbol{W} \otimes \boldsymbol{D}_{N_{SC}})\, \boldsymbol{x} \ . \end{aligned} \tag{2}$$

$\boldsymbol{W}$ originates from an LTE-A specific finite set of possible precoding matrices, called codebook [8]. The best suited matrix out of this set is obtained via the third feedback parameter, the precoding matrix indicator (PMI). The output of this transformation is then processed by N_T OFDM modulators, which apply IFFT operations of size $N_{FFT} > N_{SC}$. This can be compactly written as

$$\boldsymbol{s} = \left(\boldsymbol{I}_{N_T} \otimes \boldsymbol{P}_{\text{addCP}} \boldsymbol{D}^H_{N_{FFT}} \boldsymbol{M}\right) \boldsymbol{x}'' \ , \tag{3}$$

where

$$\boldsymbol{P}_{\text{addCP}} = \begin{pmatrix} \boldsymbol{0} & \boldsymbol{I}_{N_{CP}} \\ & \boldsymbol{I}_{N_{FFT}} \end{pmatrix}, \quad \boldsymbol{M} = \begin{pmatrix} \boldsymbol{0} \\ \boldsymbol{I}_{N_{SC}} \\ \boldsymbol{0} \end{pmatrix}$$

describes the addition of the CP of length N_{CP} and the localized subcarrier mapping of the N_{SC} subcarriers to the center of N_{FFT} DFT points, respectively. The stacked transmit signal $\boldsymbol{s}$ is described via a matrix multiplication of the stacked data vector $\boldsymbol{x}$

$$\boldsymbol{s} = \left(\boldsymbol{I}_{N_T} \otimes \boldsymbol{P}_{\text{addCP}} \boldsymbol{D}^H_{N_{FFT}} \boldsymbol{M}\right) (\boldsymbol{W} \otimes \boldsymbol{D}_{N_{SC}})\, \boldsymbol{x} \ . \tag{4}$$

Channel

The CIR from transmit antenna t to receive antenna r is denoted by $\boldsymbol{h}_{r,t}$. $\boldsymbol{H}_{r,t} = \mathrm{Toeplitz}(\boldsymbol{h}_{r,t})$ is the corresponding time domain channel matrix, which leads to the full MIMO time domain channel matrix $\boldsymbol{H} \in \mathbb{C}^{(N_{FFT}+N_{CP})N_R \times (N_{FFT}+N_{CP})N_T}$,

$$\boldsymbol{H} = \begin{pmatrix} \boldsymbol{H}_{1,1} & \ldots & \boldsymbol{H}_{1,N_T} \\ \vdots & \ddots & \vdots \\ \boldsymbol{H}_{N_R,1} & \ldots & \boldsymbol{H}_{N_R,N_T} \end{pmatrix} \ . \tag{5}$$

The received signal is corrupted by additive zero mean, i.i.d. Gaussian noise $\boldsymbol{n}$, $\mathbb{E}\{\boldsymbol{n}\boldsymbol{n}^H\} = \sigma_n^2 \boldsymbol{I}_{N_{FFT}+N_{CP}}$,

$$\boldsymbol{r} = \boldsymbol{H}\boldsymbol{s} + \boldsymbol{n} \ . \tag{6}$$

If the CP length is properly chosen, adding and removing the CP will turn the block-wise Toeplitz structure into a block-wise circulant one, given by

$$\boldsymbol{H}_{\text{cir}} = (\boldsymbol{I}_{N_R} \otimes \boldsymbol{P}_{\text{remCP}})\, \boldsymbol{H}\, (\boldsymbol{I}_{N_T} \otimes \boldsymbol{P}_{\text{addCP}}) \ . \tag{7}$$

As the columns of the DFT matrix are the eigenvectors of a circulant matrix, $\boldsymbol{H}_{cir}$ gets block-wise diagonalized by the

ISBN 978-3-8007-3662-1

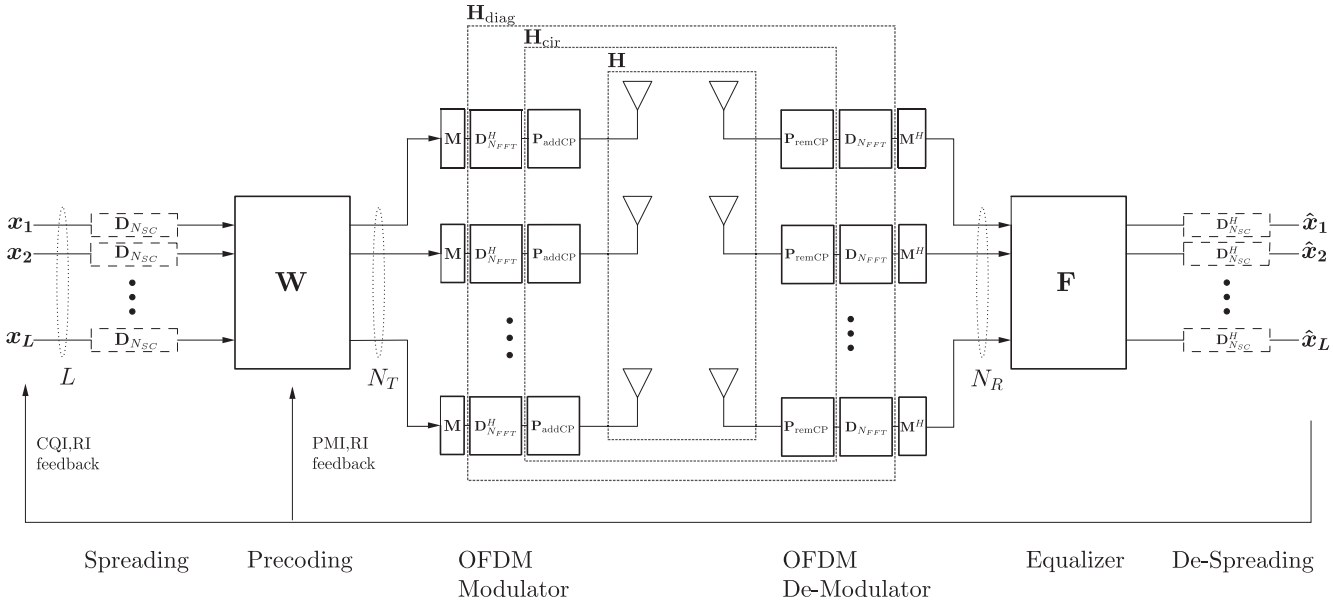

Fig. 3: Block diagram of a MIMO SC-FDMA / OFDM transmitter.

DFT/IDFT operations. The values at the block-wise diagonals are the Fourier transform of the CIR,

$$\boldsymbol{H}_{\text{diag}} = \left(\boldsymbol{I}_{N_R} \otimes \boldsymbol{D}_{N_{FFT}}\right) \boldsymbol{H}_{cir} \left(\boldsymbol{I}_{N_T} \otimes \boldsymbol{D}^H_{N_{FFT}}\right) \tag{8}$$

$$= \begin{pmatrix} \text{Diag}\left(\boldsymbol{D}_{N_{FFT}} \boldsymbol{h}_{1,1}\right) & \dots & \text{Diag}\left(\boldsymbol{D}_{N_{FFT}} \boldsymbol{h}_{1,N_T}\right) \\ \vdots & \ddots & \vdots \\ \text{Diag}\left(\boldsymbol{D}_{N_{FFT}} \boldsymbol{h}_{N_R,1}\right) & \dots & \text{Diag}\left(\boldsymbol{D}_{N_{FFT}} \boldsymbol{h}_{N_R,N_T}\right) \end{pmatrix}.$$

By incorporating the precoder in the channel, we obtain the effective channel located between the spreading and the equalizer

$$\boldsymbol{H}_{\text{eff}} = \boldsymbol{H}_{\text{diag}} \left(\boldsymbol{W} \otimes \boldsymbol{I}_{N_{SC}}\right) \ . \tag{9}$$

In case that the CP is not chosen long enough, the channel matrix will not become block-circulant after the DFT/IDFT operations as shown in Figure 4a and ISI and ICI will occur. This matrix can therefore not be diagonalized by DFT/IDFT operations as the off diagonal elements in Figure 4b illustrate.

Receiver

The OFDM demodulation consists of CP removal $\boldsymbol{P}_{\text{remCP}} = \begin{pmatrix} \boldsymbol{0} & \boldsymbol{I}_{N_{FFT}} \end{pmatrix}$ and an FFT followed by the sub-carrier de-mapping $\boldsymbol{I}_{N_R} \otimes \boldsymbol{M}^H$

$$\boldsymbol{r}'' = \left(\boldsymbol{I}_{N_R} \otimes \boldsymbol{M}^H \boldsymbol{D}_{N_{FFT}} \boldsymbol{P}_{\text{remCP}}\right) \boldsymbol{r}. \tag{10}$$

The consecutive equalizer $\boldsymbol{F}$ is generally of size $\boldsymbol{F} \in \mathbb{C}^{LN_{SC} \times N_R N_{SC}}$, which would be computationally rather complex

$$\boldsymbol{r}''' = \boldsymbol{F} \boldsymbol{r}'' \ . \tag{11}$$

By making use of the channel properties, the equalizer takes on a block-wise diagonal structure (one tap equalizer)

$$\boldsymbol{F} = \begin{pmatrix} \boldsymbol{F}_{1,1} & \dots & \boldsymbol{F}_{1,N_R} \\ \vdots & & \vdots \\ \boldsymbol{F}_{L,1} & \dots & \boldsymbol{F}_{L,N_R} \end{pmatrix} \ . \tag{12}$$

After the equalizer the layerwise spreading is removed

$$\hat{\boldsymbol{x}} = \left(\boldsymbol{I}_L \otimes \boldsymbol{D}^H_{N_{SC}}\right) \boldsymbol{r}''' = \left(\boldsymbol{I}_L \otimes \boldsymbol{D}^H_{N_{SC}}\right) \boldsymbol{F} \boldsymbol{r}'' \ . \tag{13}$$

Full System Model

The data estimates $\hat{\boldsymbol{x}}$ of the noisy received signal are

$$\begin{aligned} \hat{\boldsymbol{x}} = &\left(\boldsymbol{I}_L \otimes \boldsymbol{D}^H_{N_{SC}}\right) \boldsymbol{F} \left(\boldsymbol{I}_{N_R} \otimes \boldsymbol{M}^H \boldsymbol{D}_{N_{FFT}} \boldsymbol{P}_{\text{remCP}}\right) \boldsymbol{H} \\ &\left(\boldsymbol{I}_{N_T} \otimes \boldsymbol{P}_{\text{addCP}} \boldsymbol{D}^H_{N_{FFT}} \boldsymbol{M}\right) \left(\boldsymbol{W} \otimes \boldsymbol{D}_{N_{SC}}\right) \boldsymbol{x} \\ &+ \underbrace{\left(\boldsymbol{I}_L \otimes \boldsymbol{D}^H_{N_{SC}}\right) \boldsymbol{F} \left(\boldsymbol{I}_{N_R} \otimes \boldsymbol{M}^H \boldsymbol{D}_{N_{FFT}} \boldsymbol{P}_{\text{remCP}}\right) \boldsymbol{n}}_{\tilde{\boldsymbol{n}}} \end{aligned}$$

$$= \underbrace{\left(\boldsymbol{I}_L \otimes \boldsymbol{D}^H_{N_{SC}}\right)}_{\substack{\boldsymbol{I}_{L\,N_{SC}} \\ \text{for downlink}}} \boldsymbol{F} \boldsymbol{H}_{\text{eff}} \underbrace{\left(\boldsymbol{I}_L \otimes \boldsymbol{D}_{N_{SC}}\right)}_{\substack{\boldsymbol{I}_{L\,N_{SC}} \\ \text{for downlink}}} \boldsymbol{x} + \tilde{\boldsymbol{n}} \ . \tag{14}$$

The (uplink) solution for the ZF equalizer can be seen very easily as the spreading/de-spreading cancels if $\boldsymbol{F}\boldsymbol{H}_{\text{eff}}$ becomes the identity; thus the uplink equalizer is equal to the downlink one. As shown in Appendix A, the same holds true for the MMSE equalizer. For the remainder of the paper, we restrict ourselves to the ZF receiver in order to avoid unnecessary ambiguity with the interference term.

ISBN 978-3-8007-3662-1

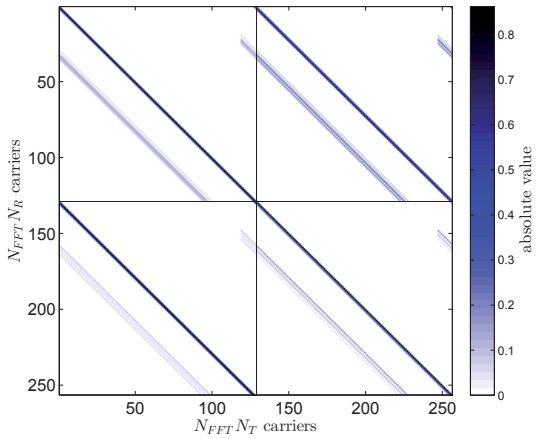

(a) Almost block-circulant channel matrix.

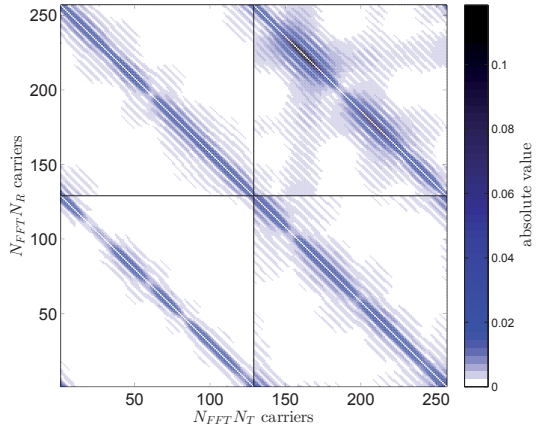

(b) Almost block-diagonal channel matrix.

Fig. 4: HT channel after the CP insertion/removal and the off-diagonal elements after the DFT/IDFT operation.

A. Uplink SNR

After the OFDM demodulation, the equalization and the de-spreading take place. The initially zero mean, i.i.d. Gaussian noise $\boldsymbol{n}$ is transformed to

$$\tilde{\boldsymbol{n}} = \left(\boldsymbol{I}_L \otimes \boldsymbol{D}_{N_{SC}}^H\right) \boldsymbol{F} \left(\boldsymbol{I}_{N_R} \otimes \boldsymbol{M}^H \boldsymbol{D}_{N_{FFT}} \boldsymbol{P}_{\text{remCP}}\right) \boldsymbol{n} \ . \tag{15}$$

As the whole processing chain is linear, the noise remains zero mean Gaussian but with a transformed covariance

$$\mathbb{E}\{\tilde{\boldsymbol{n}}\tilde{\boldsymbol{n}}^H\} = \sigma_n^2 \left(\boldsymbol{I}_L \otimes \boldsymbol{D}_{N_{SC}}^H\right) \boldsymbol{F}\boldsymbol{F}^H \left(\boldsymbol{I}_L \otimes \boldsymbol{D}_{N_{SC}}\right) \ . \tag{16}$$

Since $\boldsymbol{F}$ is a block-diagonal matrix, $\boldsymbol{F}\boldsymbol{F}^H$ is block-diagonal as well

$$\boldsymbol{F}\boldsymbol{F}^H = \begin{pmatrix} \sum_{r=1}^{N_R} \boldsymbol{F}_{1,r}\boldsymbol{F}_{1,r}^H & \cdots & \sum_{r=1}^{N_R} \boldsymbol{F}_{1,r}\boldsymbol{F}_{l,r}^H & \cdots & \sum_{r=1}^{N_R} \boldsymbol{F}_{1,r}\boldsymbol{F}_{L,r}^H \\ \vdots & & \sum_{r=1}^{N_R} \boldsymbol{F}_{l,r}\boldsymbol{F}_{l,r}^H & & \vdots \\ \sum_{r=1}^{N_R} \boldsymbol{F}_{L,r}\boldsymbol{F}_{1,r}^H & \cdots & \sum_{r=1}^{N_R} \boldsymbol{F}_{L,r}\boldsymbol{F}_{l,r}^H & \cdots & \sum_{r=1}^{N_R} \boldsymbol{F}_{L,r}\boldsymbol{F}_{L,r}^H \end{pmatrix} . \tag{17}$$

Due to the DFT multiplication from the left and the right, the covariance matrix will be of block-circulant structure, cf. (18). As shown in Appendix B, the diagonal elements calculate to

$$\boldsymbol{\sigma}_{\tilde{\boldsymbol{n}}}^2 = \text{diag}\left(\mathbb{E}\{\tilde{\boldsymbol{n}}\tilde{\boldsymbol{n}}^H\}\right) \tag{19}$$

$$= \frac{\sigma_n^2}{N_{SC}} \begin{pmatrix} \left(\sum_{k=1}^{N_{SC}} \sum_{r=1}^{N_R} \boldsymbol{F}_{1,r}[k,k]\boldsymbol{F}_{1,r}^H[k,k]\right) \mathbb{1}_{N_{SC}} \\ \vdots \\ \left(\sum_{k=1}^{N_{SC}} \sum_{r=1}^{N_R} \boldsymbol{F}_{l,r}[k,k]\boldsymbol{F}_{l,r}^H[k,k]\right) \mathbb{1}_{N_{SC}} \\ \vdots \\ \left(\sum_{k=1}^{N_{SC}} \sum_{r=1}^{N_R} \boldsymbol{F}_{L,r}[k,k]\boldsymbol{F}_{L,r}^H[k,k]\right) \mathbb{1}_{N_{SC}} \end{pmatrix}$$

$$= \frac{\sigma_n^2}{N_{SC}} \begin{pmatrix} \|\boldsymbol{S}_1\boldsymbol{F}\|_F^2 \mathbb{1}_{N_{SC}} \\ \vdots \\ \|\boldsymbol{S}_l\boldsymbol{F}\|_F^2 \mathbb{1}_{N_{SC}} \\ \vdots \\ \|\boldsymbol{S}_L\boldsymbol{F}\|_F^2 \mathbb{1}_{N_{SC}} \end{pmatrix} , \tag{20}$$

where

$$\boldsymbol{S}_l = (\boldsymbol{0}_{N_{SC}} \ldots \boldsymbol{0}_{N_{SC}} \boldsymbol{I}_{N_{SC}} \boldsymbol{0}_{N_{SC}} \ldots \boldsymbol{0}_{N_{SC}}) \ , \tag{21}$$

is selecting the relevant components for layer l with the identity matrix at the lth position. In analogy to [9], in uplink transmission - due to the DFT pre-spreading applied with SC-FDMA - the SNR is constant over all subcarriers (note that there is no subcarrier index k involved)

$$\text{SNR}_l^{UL} = \frac{N_{SC}\sigma_x^2}{\sigma_n^2 \|\boldsymbol{S}_l\boldsymbol{F}\|_F^2} \ , \tag{22}$$

with the matrix $\boldsymbol{S}_l$ selecting only that part of the equalizer which has impact on layer l and σ_x^2 denoting the transmit power.

B. Downlink SNR

The equalizer runs on a subcarrrier level where it has to equalize the MIMO channel $\boldsymbol{H}_{\text{eff}}$. In contrast to the uplink, no spreading takes place in the downlink transmission, thus the different subcarriers k are independent and the equalizer has only to deal with the subcarrier channel $\boldsymbol{H}_k$. We use the subscript k to denote the relevant part of the full channel matrix for the kth subcarrier. The corresponding indices within the diagonal matrix $\boldsymbol{H}_{\text{diag}}$ are $\mathbb{1}_{N_R \times N_T} \otimes \text{Diag}\,(\boldsymbol{e}_k)$, with the canonical base vectors $\boldsymbol{e}_k$. Using this notation, the subcarrier channel $\boldsymbol{H}_{\text{eff},k}$ is

$$\boldsymbol{H}_{\text{eff},k} = \boldsymbol{H}_{\text{diag}} \left[\mathbb{1}_{N_R \times N_T} \otimes \text{Diag}\,(\boldsymbol{e}_k)\right] \boldsymbol{W} \ , \tag{23}$$

and $\boldsymbol{F}_k$ is its ZF equalizer. The SNR formula is quite similar to the uplink case, except that the SNR shows subcarrier dependency now

$$\mathbf{SNR}_l^{DL}[k] = \frac{\sigma_x^2}{\sigma_n^2 \|\boldsymbol{S}_l'\boldsymbol{F}_k\|_F^2} \ . \tag{24}$$

The selection matrix $\boldsymbol{S}_l'$ is built as

$$\boldsymbol{S}_l' = (\ \boldsymbol{0} \quad \mathbb{1}_{N_R} \quad \boldsymbol{0}\ )^T \ , \tag{25}$$

with appropriate zero matrices $\boldsymbol{0}$ and the all ones vector $\mathbb{1}_{N_R}$ at the lth row.

ISBN 978-3-8007-3662-1

$$\mathbb{E}\{\tilde{\boldsymbol{n}}\tilde{\boldsymbol{n}}^H\} = \sigma_n^2 \begin{pmatrix} \boldsymbol{D}_{N_{SC}}^H \sum_{r=1}^{N_R} \boldsymbol{F}_{1,r}\boldsymbol{F}_{1,r}^H \boldsymbol{D}_{N_{SC}} & \dots & \boldsymbol{D}_{N_{SC}}^H \sum_{r=1}^{N_R} \boldsymbol{F}_{1,r}\boldsymbol{F}_{l,r}^H \boldsymbol{D}_{N_{SC}} & \dots & \boldsymbol{D}_{N_{SC}}^H \sum_{r=1}^{N_R} \boldsymbol{F}_{1,r}\boldsymbol{F}_{L,r}^H \boldsymbol{D}_{N_{SC}} \\ \vdots & & \boldsymbol{D}_{N_{SC}}^H \sum_{r=1}^{N_R} \boldsymbol{F}_{l,r}\boldsymbol{F}_{l,r}^H \boldsymbol{D}_{N_{SC}} & & \vdots \\ \boldsymbol{D}_{N_{SC}}^H \sum_{r=1}^{N_R} \boldsymbol{F}_{L,r}\boldsymbol{F}_{1,r}^H \boldsymbol{D}_{N_{SC}} & \dots & \boldsymbol{D}_{N_{SC}}^H \sum_{r=1}^{N_R} \boldsymbol{F}_{L,r}\boldsymbol{F}_{l,r}^H \boldsymbol{D}_{N_{SC}} & \dots & \boldsymbol{D}_{N_{SC}}^H \sum_{r=1}^{N_R} \boldsymbol{F}_{L,r}\boldsymbol{F}_{L,r}^H \boldsymbol{D}_{N_{SC}} \end{pmatrix} \tag{18}$$

III. ISI/ICI MODELLING

In [10] results were established for ISI/ICI due to insufficient CP length in a discrete multi tone (OFDM) setting, which were extended to SISO SC-FDMA in [9]. We now extend this theory to MIMO, for both SC-FDMA and OFDM.
In [9], we have also demonstrated that the frequency selectivity of the ISI/ICI has a great dynamical range, which was further pronounced by the equalizer. Simulations show a similar frequency selectivity in the MIMO case, cf. Figure 5.
The antennas are linear combiners so that similar to [10], the ISI can be expressed via convolution

$$\begin{aligned} \boldsymbol{r}'_{\mathrm{ISI^{CP}},r}[k] &= \boldsymbol{r}'_{I,r}[k] = \sum_{t=1}^{N_T} \sum_{n=0}^{N_{SC}-1} \sum_{\substack{\nu= \\ N_{CP}+1+n}}^{N_h-1} \boldsymbol{h}_{r,t}[\nu]\, \tilde{\boldsymbol{s}}_t[n-\nu] e^{-j\frac{2\pi}{K}nk} \\ &= \sum_{t=1}^{N_T} \sum_{\substack{m= \\ N_{CP}+1}}^{N_h-1} \boldsymbol{s}_t[-m] e^{j\frac{2\pi}{N}mk} \boldsymbol{\mathcal{H}}_{r,t}[m,k] \ , \end{aligned} \tag{26}$$

where we applied the abbreviation

$$\boldsymbol{\mathcal{H}}_{r,t}[m,k] = \sum_{q=m}^{N_h-1} \boldsymbol{h}_{r,t}[q]\, e^{-j\frac{2\pi}{N_{FFT}}qk} \tag{27}$$

for the DFT of the channel impulse's tail and $\tilde{\boldsymbol{s}}_t$ denotes the concatenation of the past and the present symbols at transmit antenna t. The ICI calculates to

$$\boldsymbol{r}'_{\mathrm{ICI^{CP}},r}[k] = -\sum_{t=1}^{N_T} \sum_{n=0}^{N_h-1-N_{SC}} \sum_{\substack{\nu= \\ N_{SC}+n+1}}^{N_h-1} \boldsymbol{h}_{r,t}[\nu]\, \boldsymbol{s}_t[(n-\nu) \bmod N] e^{-j\frac{2\pi}{K}nk} \ , \tag{28}$$

with the current OFDM symbol $\boldsymbol{s}_t$ on transmit antenna t. As it leads to the same PSD as the occuring ISI [11], we will derive only the PSD of the ISI in the following, which will be augmented by a factor of two in a last step, in order to account for the ICI.
We start from the definition of the PSD of a weak sense stationary random process $\boldsymbol{x}$

$$S_x(e^{j\theta}) = \lim_{N\to\infty} \mathbb{E}\left\{ \frac{1}{N} \left| \sum_{n=1}^{N} x[n] e^{-j\theta n} \right|^2 \right\} . \tag{29}$$

Sampling in the frequency space, i.e., $\theta = \frac{2\pi k}{N}$, $k = 1,\dots,N$, and omitting the limit leads to the following averaged periodogram of the PSD

$$\boldsymbol{N}_x[k] = \mathbb{E}\left\{ \frac{1}{N} \left| \sum_{n=1}^{N} x[n] e^{-j\frac{2\pi k}{N}n} \right|^2 \right\} = \frac{1}{N}\mathbb{E}\left\{ |X[k]|^2 \right\} . \tag{30}$$

For the feedback we are interested in the post equalization (post de-spreading) SINR and we therefore need to include the equalizer into the PSD calculation

$$\boldsymbol{r}'''_I = \boldsymbol{F}(\boldsymbol{I}_R \otimes \boldsymbol{M}^H)\boldsymbol{r}'_I \ \Rightarrow\ \boldsymbol{N}_{r'''_I}[k] = \mathbb{E}\left\{ |\boldsymbol{r}'''_I[k]|^2 \right\} . \tag{31}$$

We use $\tilde{k} = k + (N_{FFT} - N_{SC})/2$ to describe the action of the subcarrier mapping $\boldsymbol{M}$ where $\tilde{k}$ picks out the N_{SC} middle subcarriers, i.e., $\tilde{k} \in \{\frac{N_{FFT}-N_{SC}}{2}, \dots, \frac{N_{FFT}+N_{SC}}{2}\}$. The PSD component on the lth layer at subcarrier k is therefore described by

$$\begin{aligned} &\boldsymbol{N}_{r'''_I,l}[k] \\ &= \mathbb{E}\left\{ \left| \boldsymbol{F}_{l,1}[k,k]\boldsymbol{r}'_{I,1}[\tilde{k}] + \dots + \boldsymbol{F}_{l,N_R}[k,k]\boldsymbol{r}'_{I,N_R}[\tilde{k}] \right|^2 \right\} \\ &= \sum_{r_i=1}^{N_R} \sum_{r_j=1}^{N_R} \boldsymbol{F}_{l,r_i}[k,k] \mathbb{E}\left\{ \boldsymbol{r}'_{I,r_i}[\tilde{k}] (\boldsymbol{r}'_{I,r_j}[\tilde{k}])^* \right\} \boldsymbol{F}^*_{l,r_j}[k,k] \ . \end{aligned} \tag{32}$$

Next we derive the expectation terms

$$\begin{aligned} &\mathbb{E}\left\{ \boldsymbol{r}'_{I,r_i}[\tilde{k}] (\boldsymbol{r}'_{I,r_j}[\tilde{k}])^* \right\} \\ &= \mathbb{E}\left\{ \sum_{t_1=1}^{N_T} \sum_{\substack{m_1= \\ N_{CP}+1}}^{N_h-1} \boldsymbol{s}_{t_1}[-m_1] e^{j\frac{2\pi}{N}m_1\tilde{k}} \boldsymbol{\mathcal{H}}_{r_i,t_1}[m_1,\tilde{k}] \right. \\ &\qquad \left. \sum_{t_2=1}^{N_T} \sum_{\substack{m_2= \\ N_{CP}+1}}^{N_h-1} \boldsymbol{s}^*_{t_2}[-m_2] e^{-j\frac{2\pi}{N}m_2\tilde{k}} \boldsymbol{\mathcal{H}}^*_{r_j,t_2}[m_2,\tilde{k}] \right\} \\ &= \sum_{t_1=1}^{N_T} \sum_{\substack{m_1= \\ N_{CP}+1}}^{N_h-1} \sum_{t_2=1}^{N_T} \sum_{\substack{m_2= \\ N_{CP}+1}}^{N_h-1} \boldsymbol{\mathcal{H}}_{r_i,t_1}[m_1,\tilde{k}] \boldsymbol{\mathcal{H}}^*_{r_j,t_2}[m_2,\tilde{k}] \\ &\qquad \mathbb{E}\left\{ \boldsymbol{s}_{t_1}[-m_1] \boldsymbol{s}^*_{t_2}[-m_2] \right\} e^{-j\frac{2\pi}{N}(m_2-m_1)\tilde{k}} \ . \end{aligned} \tag{33}$$

For white data the expectation is zero if $m_1 \neq m_2 = m$, so that the sums over m_1, m_2 collapse into one.
The same idea is used for the expectation across the transmit antennas. If $t_1 \neq t_2 = t$ the expectation is *approximated* by zero. For LTE-A precoders this approximation is sufficiently well fulfilled in a 2×2 system. However, due to limited number of code words in LTE-A [8], it is not fulfilled in larger MIMO systems and the correlation between transmit antennas should be taken into account. Despite this approximation error, the simulation results are satisfactory, and we can avoid the additional signalling of the codeword to layer mapping and the used precoder. With this assumptions we are now able to

ISBN 978-3-8007-3662-1

write

$$\mathbb{E}\left\{\boldsymbol{r}'_{r_i}[\tilde{k}](\boldsymbol{r}'_{r_j}[\tilde{k}])^*\right\} \tag{34}$$
$$= \sum_{t=1}^{N_T} \sum_{\substack{m= \\ N_{CP}+1}}^{N_h-1} \boldsymbol{\mathcal{H}}_{r_i,t}[m,\tilde{k}]\boldsymbol{\mathcal{H}}^*_{r_j,t}[m,\tilde{k}] \underbrace{\mathbb{E}\left\{\boldsymbol{s}_t[-m]\boldsymbol{s}^*_t[-m]\right\}}_{\sigma^2_{s_t}=\sigma^2_x}$$
$$= \sigma^2_x \sum_{t=1}^{N_T} \boldsymbol{\mathcal{H}}^H_{r_j,t}[:,\tilde{k}]\boldsymbol{\mathcal{H}}_{r_i,t}[:,\tilde{k}] \ .$$

The operator ' : ' takes all elements and is inspired by MATLAB's syntax. The equality $\sigma^2_{s_t} = \sigma^2_x$ hold true for a semi-unitary precoder $\boldsymbol{W}$, which is the case for the LTE-A codebook. We arrive at the kth PSD component at the lth layer

$$\boldsymbol{N}_{r'''_I,l}[k] \tag{35}$$
$$= \sigma^2_x \sum_{r_i=1}^{N_R}\sum_{r_j=1}^{N_R} \boldsymbol{F}_{l,r_i}[k,k]\left(\sum_{t=1}^{N_T}\boldsymbol{\mathcal{H}}^H_{r_j,t}[:,\tilde{k}]\boldsymbol{\mathcal{H}}_{r_i,t}[:,\tilde{k}]\right)\boldsymbol{F}^*_{l,r_j}[k,k] \ .$$

The whole PSD vector can be expresssed as shown in (36).

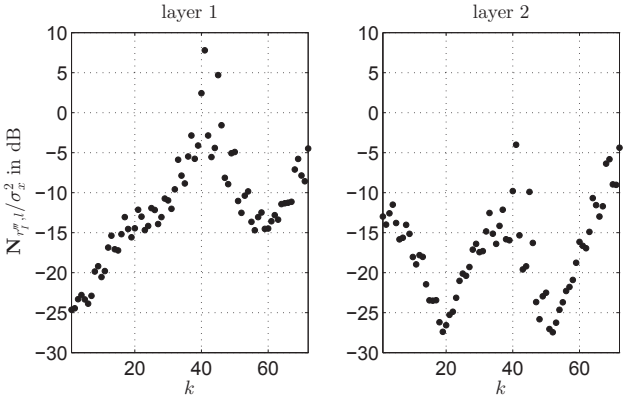

Fig. 5: Simulated ISI/ICI PSD after equalization for one HT channel realization.

A. Uplink

A stationary random process (the ISI/ICI), where all moments exist, is asympotically ($N_{SC} \to \infty$) independent complex Gaussian distributed after a finite Fourier transform (de-spreading) and the variances are equal to the PSD before the IDFT [12]. This helpful theorem allows us to model the interference caused by the insufficient CP length as coloured Gaussian noise

$$\boldsymbol{\sigma}^2_{I,l} = 2\boldsymbol{N}_{r'''_I,l} \ , \tag{37}$$

where the factor of two accounts for the effect of the ISI and ICI power as previously mentioned.

B. Downlink

As the downlink does not apply spreading and de-spreading, the ISI/ICI distribution is not Gaussian in general and (37) does not hold true. The random process is zero mean, thus a variance fit is the best fit up to second-order moments, and the approximation

$$\boldsymbol{\sigma}^2_{I,l} \approx 2\boldsymbol{N}_{r'''_I,l} \tag{38}$$

yields satisfactory results.

IV. Feedback Parameter Calculation

Utilizing the SINR, which is determined by the interference modelled as coloured noise $\boldsymbol{\sigma}^2_{I,l}$ together with the enhanced noise, we calculate the feedback parameters applying methods from [13]. The uplink expression is now, in contrast to the SNR, frequency dependent

$$\mathbf{SINR}^{UL}_l[k] = \frac{N_{SC}\sigma^2_x}{N_{SC}\boldsymbol{\sigma}^2_{I,l}[k] + \sigma^2_n\|\boldsymbol{S}_l\boldsymbol{F}\|^2_F} \ . \tag{39}$$

The downlink SINR is again a special case and calculates to

$$\mathbf{SINR}^{DL}_l[k] = \frac{\sigma^2_x}{\boldsymbol{\sigma}^2_{I,l}[k] + \sigma^2_n\|\boldsymbol{S}'_l\boldsymbol{F}_k\|^2_F} \ . \tag{40}$$

V. Simulations

Our simulations were carried out by the Vienna LTE-A Uplink/Downlink Link Level simulators [14], [15], [16] applying the HT channel model and simulation parameters as given in Table I. The delay spread of the channel model is about three times longer than LTE's normal CP length, cf. Fig. 2. As mentioned before, this can either model a large cell with a scatterer in great distance, or equivalently, an SFN environment.

In all our simulations we employed a single base station and a single user in order to focus on the physical layer effects, although [17], [18] have shown that frequency selective scheduling leads to throughput enhancement.

Simulation results for a 2×2 MIMO LTE-A uplink transmission, a 2×2 downlink transmission and a 4×4 downlink transmission are shown in Figure 6, Figure 7 and Figure 8, respectively. Our proposed feedback method, which takes the occurring ISI and ICI into account is indicated by solid lines and referred to as *interference aware feedback*. In dashed lines, the throughput obtained with *interference ignorant feedback* is shown. Results obtained using normal CP length or extended CP length are drawn in red and blue, respectively.

In case of normal CP length with *interference ignorant feedback*, the strong occurring ISI and ICI deteriorates the system's performance significantly. Ignoring the ISI/ICI in the feedback parameter calculation results in a too optimistic feedback and the therefore applied MCS is not suited for the actual channel state. The performance of employing an extended CP together with *interference ignorant feedback*, as a straightforward solution in LTE-A, is given by the solid blue curve. It is able to circumvent the occurrence of ISI and ICI but suffers from the fact that only 12 instead of 14 OFDM symbols can be used in a subframe. This throughput loss of 1/7 is independent of the actually occurring ISI and ICI, and can be seen in the low SNR region. However, the delay spread of the HT channel exceeds even the extended CP, so that the *interference aware* feedback can further improve the performance when the extended CP is used.

In our simulation scenario all $N_T \times N_R$ CIRs have an HT power delay profile and there is no correlation between the

ISBN 978-3-8007-3662-1

$$\boldsymbol{N}_{r_I''',l} = \mathbb{E}\left\{\mathrm{diag}\left((\boldsymbol{F}_{l,1}\boldsymbol{M}^H\boldsymbol{r}'_1 + \cdots + \boldsymbol{F}_{l,N_R}\boldsymbol{M}^H\boldsymbol{r}'_{N_R})(\boldsymbol{F}_{l,1}\boldsymbol{M}^H\boldsymbol{r}'_1 + \cdots + \boldsymbol{F}_{l,N_R}\boldsymbol{M}^H\boldsymbol{r}'_{N_R})^H\right)\right\}$$
$$= \sigma_x^2\,\mathrm{diag}\left(\sum_{r_i=1}^{N_R}\sum_{r_j=1}^{N_R}\boldsymbol{F}_{l,r_i}\boldsymbol{M}^H\left(\boldsymbol{I}_{N_{FFT}}\odot\left(\sum_{t=1}^{N_T}\boldsymbol{\mathcal{H}}_{r_j,t}^H\boldsymbol{\mathcal{H}}_{r_i,t}\right)\right)\boldsymbol{M}\boldsymbol{F}_{l,r_j}^H\right) \quad (36)$$

TABLE I: Simulation Parameters

Parameter	Value
System bandwidth	1.4MHz
Number of subcarriers N_{SC}	72
Feedback	interference ignorant / aware
Feeback delay	0 TTI
Feedback cluster size	72 (full bandwidth)
Channel model	HT [1]
Antenna configuration	2×2 uplink / downlink
	4×4 downlink
Receiver	Zero Forcing (ZF)
Channel estimator	perfect channel knowledge
CP length	normal / extended

transmit and receive antennas (iid model). The 4×4 system with 16 exceeding channel delay spreads is more sensitive to occurring ISI/ICI, so that our proposed method shows tremendous improvements between 5 and 15dB SNR compared to extended CP versions. At 10dB the throughput obtained with the interference aware feedback and normal CP is approximately twice as much as obtained with an employed extended CP.

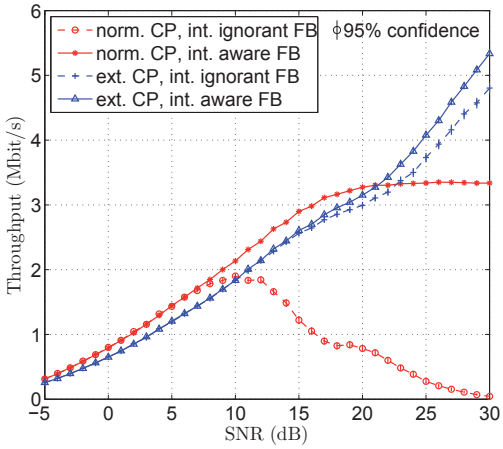

Fig. 6: Uplink throughput for a 2×2 MIMO transmission.

VI. Conclusion

In order to capture additional delay spread in MBSFN transmissions, typically extended CPs are being employed [19]. However, the extended CP leads to a capacity loss irrespective of the actual shape of the CIR. Our proposed, interference aware, feedback method applies the normal CP length in order to avoid the described loss of throughput. We combat the effects of insufficient CP length by adapting the MCS via feedback. This is achieved by taking the occurring ISI and ICI into account in the SINR calculation, which is exploited

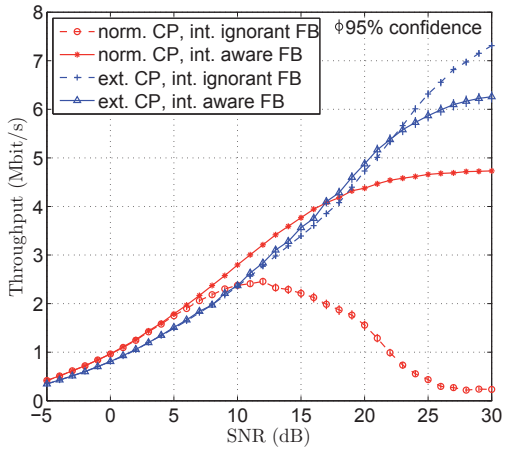

Fig. 7: Downlink throughput for a 2×2 MIMO transmission.

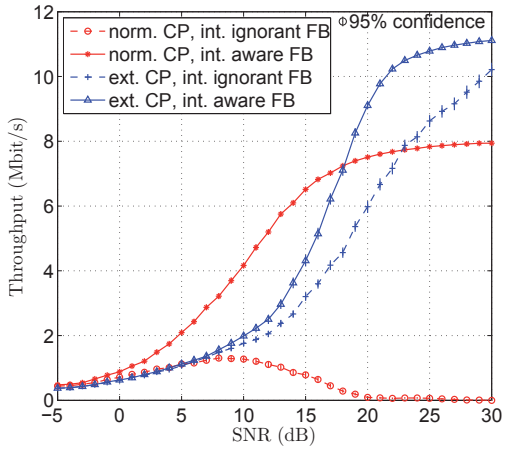

Fig. 8: Downlink throughput for a 4×4 MIMO transmission.

for determining the feedback parameters. With this method we achieve a higher throughput than using the extended CP, in a reasonable SNR region. As our method is not an either-or decision, it can be applied in addition to existing ISI and ICI mitigation methods e.g., the extended CP. Keeping in mind, that the used channel model has an extremely large delay spread, it might not be beneficial to use the extended CP length on other channels at all. Our interference aware feedback method can improve the performance without increasing the CP length and make the decision, when to use the extended CP length, obsolete.

ISBN 978-3-8007-3662-1

APPENDIX A - MMSE EQUALIZER

We start from (14) and calculate the MMSE optimal equalizer $\boldsymbol{F}$ as

$$\begin{aligned}
&\boldsymbol{F}_{\mathrm{MMSE}} = \\
&= \underset{\boldsymbol{F}}{\operatorname{argmin}}\, \mathbf{E}\{||\hat{\boldsymbol{x}} - \boldsymbol{x}||_2^2\} \\
&= \underset{\boldsymbol{F}}{\operatorname{argmin}}\, \mathbf{E}\Big\{\Big(\Big(\boldsymbol{I}_L \otimes \boldsymbol{D}_{N_{SC}}^H\Big)\boldsymbol{F}\boldsymbol{H}_{\mathrm{eff}}\left(\boldsymbol{I}_L \otimes \boldsymbol{D}_{N_{SC}}\right)\boldsymbol{x} + \tilde{\boldsymbol{n}} - \boldsymbol{x}\Big)^H \\
&\quad \Big(\Big(\boldsymbol{I}_L \otimes \boldsymbol{D}_{N_{SC}}^H\Big)\boldsymbol{F}\boldsymbol{H}_{\mathrm{eff}}\left(\boldsymbol{I}_L \otimes \boldsymbol{D}_{N_{SC}}\right)\boldsymbol{x} + \tilde{\boldsymbol{n}} - \boldsymbol{x}\Big)\Big\} \\
&= \arg\min_{\boldsymbol{F}}\ \operatorname{trace}\Big\{\sigma_x^2 \boldsymbol{F}\boldsymbol{H}_{\mathrm{eff}}\boldsymbol{H}_{\mathrm{eff}}^H\boldsymbol{F}^H \\
&\quad - \sigma_x^2\boldsymbol{H}_{\mathrm{eff}}^H\boldsymbol{F}^H - \sigma_x^2\boldsymbol{F}\boldsymbol{H}_{\mathrm{eff}} + \sigma_n^2\boldsymbol{F}\boldsymbol{F}^H\Big\}\ .
\end{aligned}$$

Minimizing this expression yields

$$\begin{aligned}
0 &= 2\sigma_x^2\boldsymbol{H}_{\mathrm{eff}}\boldsymbol{H}_{\mathrm{eff}}^H\boldsymbol{F}_{\mathrm{MMSE}}^H - 2\sigma_x^2\boldsymbol{H}_{\mathrm{eff}} + 2\sigma_n^2\boldsymbol{F}_{\mathrm{MMSE}}^H \\
\boldsymbol{F}_{\mathrm{MMSE}} &= \sigma_x^2\boldsymbol{H}_{\mathrm{eff}}^H\left(\sigma_x^2\boldsymbol{H}_{\mathrm{eff}}\boldsymbol{H}_{\mathrm{eff}}^H + \sigma_n^2\boldsymbol{I}_{N_{SC}L}\right)^{-1}\ .
\end{aligned}$$

APPENDIX B - CIRCULANT MATRICES

A circulant matrix $\boldsymbol{C} \in \mathbb{C}^{N\times N}$ is fully described by it's first column $\boldsymbol{c}$, and its eigenvalues are the DFT of $\boldsymbol{c} = (c_0, c_1, \ldots, c_{n-1})$.

$$\boldsymbol{C} = \begin{pmatrix} c_0 & c_{n-1} & \ldots & c_2 & c_1 \\ c_1 & c_0 & c_{n-1} & & c_2 \\ \vdots & c_1 & c_0 & \ddots & \vdots \\ c_{n-2} & & \ddots & \ddots & c_{n-1} \\ c_{n-1} & c_{n-2} & \ldots & c_1 & c_0 \end{pmatrix} \tag{41}$$

$$\boldsymbol{C} = \boldsymbol{D}^H \operatorname{Diag}(\boldsymbol{D}\boldsymbol{c})\boldsymbol{D} \tag{42}$$

Using the DFT matrix $\boldsymbol{D} \in \mathbb{C}^{N\times N}$, the main diagonal elements c_0 of $\boldsymbol{C}$ are given by $\frac{1}{N}\sum_i(\boldsymbol{D}\boldsymbol{c})_i$.

REFERENCES

[1] 3GPP TR25.943, *Technical specification group radio access networks; Deployment aspects (Release 12)*, http://www.3gpp.org/ftp/Specs/html-info/25943.htm, Sep. 2014.

[2] 3GPP TS25.346, *Introduction of the Multimedia Broadcast/Multicast Service (MBMS) in the Radio Access Network (RAN); Stage 2 (Release 12)*, http://www.3gpp.org/DynaReport/25346.htm, Mar. 2014.

[3] A. Zakrzewska, D. López-Pérez, S. Kucera, and H. Claussen, "Dual connectivity in LTE hetnets with split control-and user-plane," in *Globecom Workshops (GC Wkshps), 2013 IEEE*. IEEE, 2013, pp. 391–396.

[4] A. G. Burr, "Performance analysis of COFDM for broadband transmission on a fading multipath channel," *Wireless personal communications*, vol. 10, no. 1, pp. 3–17, 1999.

[5] A. Gusmao, P. Torres, R. Dinis, and N. Esteves, "A turbo FDE technique for reduced-CP SC-based block transmission systems," *IEEE Transactions on Communications*, vol. 55, no. 1, pp. 16–20, Jan. 2007.

[6] C. Mehlführer, S. Caban, and M. Rupp, "Cellular system physical layer throughput: How far off are we from the Shannon bound?" *IEEE Wireless Communications Magazine*, vol. 18, no. 6, pp. 54–63, Dec. 2011.

[7] A. Wilzeck, Q. Cai, M. Schiewer, and T. Kaiser, "Effect of multiple carrier frequency offsets in MIMO SC-FDMA systems," in *Proceedings of the International ITG/IEEE Workshop on Smart Antennas*, 2007.

[8] 3GPP TS36.211, *Technical specification group radio access networks; Physical Channels and Modulation (Release 12)*, http://www.3gpp.org/DynaReport/36211.htm, Sep. 2014.

[9] E. Zöchmann, S. Pratschner, S. Schwarz, and M. Rupp, "Limited feedback in OFDM systems for combating ISI/ICI caused by insufficient cyclic prefix length," in *Proc. IEEE Asilomar Conf. on Signals, Systems, and Comp.*, Nov. 2014.

[10] W. Henkel, G. Tauböck, P. Ödling, P. Börjesson, and N. Petersson, "The cyclic prefix of OFDM/DMT - an analysis," in *International Zurich Seminar on Broadband Communications, Access, Transmission, Networking*, Zurich, February 2002, pp. 22–1 – 22–3.

[11] G. Tauböck, "Wireline Multiple Input / Multiple Output Systems," Doctoral Thesis (Electrical Engineering), Vienna University of Technology, Vienna, 2005, http://www.nt.tuwien.ac.at/fileadmin/users/gtauboec/diss_tauboeck.pdf.

[12] D. R. Brillinger, *Time series: data analysis and theory*. McGraw-Hill, 1981.

[13] S. Schwarz, C. Mehlführer, and M. Rupp, "Calculation of the spatial preprocessing and link adaption feedback for 3GPP UMTS/LTE," in *6th Conference on Wireless Advanced (WiAD)*, London, June 2010, pp. 1–6.

[14] S. Schwarz, J. Ikuno, M. Simko, M. Taranetz, Q. Wang, and M. Rupp, "Pushing the limits of LTE: A survey on research enhancing the standard," *IEEE Access*, vol. 1, pp. 51–62, 2013.

[15] [Online]. Available: http://www.nt.tuwien.ac.at/ltesimulator/

[16] J. Blumenstein, J. Ikuno, J. Prokopec, and M. Rupp, "Simulating the long term evolution uplink physical layer," in *Proceedings ELMAR*, Zadar, September 2011, pp. 141–144.

[17] S. Schwarz, C. Mehlführer, and M. Rupp, "Throughput maximizing multiuser scheduling with adjustable fairness," in *IEEE International Conference on Communications (ICC)*. IEEE, 2011, pp. 1–5.

[18] ——, "Low complexity approximate maximum throughput scheduling for LTE," in *Conference Record of the Forty Fourth Asilomar Conference on Signals, Systems, and Computers*, Pacific Grove, California, Nov. 2010, pp. 1563–1569.

[19] E. Dahlman, S. Parkvall, and J. Skold, *4G: LTE/LTE-advanced for mobile broadband*. Academic Press, 2013.

